THE ROLE OF WATER VAPOR RADIOMETERS FOR IN-FLIGHT CALIBRATION OF THE TOPEX MICROWAVE RADIOMETER

Stephen J. Keihm[1]
Christopher S. Ruf[2]

submitted to
Journal of Marine Geodesy
on
December 17, 1993

1, Jet Propulsion Laboratory, California Institute of Technology,
Pasadena, CA 91109

2. Department of Electrical Engineering, The Pennsylvania State University,
University Park, PA 16802

ABSTRACT

First year results are presented for the in-flight calibration and performance evaluation of the '1 'OPEX Microwave Radiometer ('1 'MR), based on overflight comparisons with ground-based water vapor radiometer (WVR) data. {comparisons are made in terms of both 'TMR brightness temperat ures and the retrieved range correct ion due to Tropospheric waler vapor (path delay).

Comparisons of TMR brightness temperature measurements with predictions based on WVR data and a calm sea flux model provided early recognit ion of TMR pm-night calibration errors which were not apparent based on ground truth path delay comparisons. Later comparisons, using the final TMR calibration algorithms, are used to constrain the model for the calm sea surface nadir emissivity. The results suggest that the 18-37 GHz calm sea flux is enhanced 1-2 K relative. to the predictions of a Fresnel model for a plane surface,

{'comparisons in the path delay domain illustrate the advantages of using time and space coincident ground measurements for in-flight calibration and performance monitoring, of satellite radiometer measurements. The results demonstrate that elimination of temporal and spatial decorrelation errors reduces path delay comparison residuals to less than 1 cm, in contrast to the 3 cm scatter produced by the customary radiosonde comparisons.

Keywords: '1'01'1 :X Microwave Radiometer, water vapor radiometer, wet troposphere range correction, path delay, in-flight calibration, brightness temperature

1. introduction

Altimetry measurements of sca level require a number of corrections for atmosphere-induced time delays, one of which is that caused by tropospheric water vapor and cloud liquid, This delay, expressed as a range correction (hereafter referred to as path delay), is highly variable in time and space, ranging from -- 3 cm for cold, dry conditions to 45 cm for warm, humid conditions, The '1'01'1 :X Microwave Radiometer (TMR) was included in the TOPEX/Poseidon altimetry mission to provide the path delay correction to an accuracy of 1.2 cm (Carlisle et al., 1991). 'I'he '1 'MR consists of three nadir-viewing channels (18, 21, and 37 GHz) which measure the emission (brightness temperat urc) from the at mosphere and sea surface. '1 'hc 21 GHz channel, operating near the peak of the 22.235 G] Iz water vapor absorption resonance, is the primary vapor sensing channel, The 37 GHz channel is most sensitive to liquid water and provides a measurement used to separate the liquid and vapor contributions in the presence of clouds. The 18 GHz channel provides a correction for variability in the sea surface background flux due mainly to the effects of wind on the surface emissivity. Due to the frequency proximity of the 18 and 21 GHz channels, they respond nearly equally to variations in the sca surface flux. '1'bus, variations in atmospheric water vapor abundance, and the related path delay, arc strongly correlated with the brightness temperature difference

between the 21 and 18 GHz measurements. For further details on the interpretation of the TMR measurements in terms of path delay (the "retrieval algorithm"), see Keihm et al. (1993a).

In-flight calibration of the TMR antenna temperature measurements is performed by alternately switching the radiometer input between the main antenna, a smaller antenna pointed into cold space, or to an internal matched load. The antenna temper-aturc calibration equations take into account hardware component losses and their temperature dependencies, which were determined prior to launch in a series of thermal vacuum ("T/V) tests (Ruf et al., 1993a). Error sources associated with the pre-launch antenna temperature algorithm include errors in the extrapolation from T/V simulated cold space at ~ 77 K to in-flight cold space at - 2.7 K, high order instrument non-linearities not properly modelled by the quadratic calibration algorithm, and small measurement errors in the T/V tests.

The conversion of antenna temperatures to nadir brightness temperatures requires a second calibration algorithm which takes into account side lobe contributions to the measured signals (Janssen et al., 1993). Antenna range measurements, conducted prior to launch, were used to determine beam pattern parameters which wctc included in the antenna pattern correction (APC) algorithm. 1 Error sources associated with the APC include errors in the antenna range measurements and uncertainties in the brightness temperatures viewed by the on-earth side lobes. An additional potential source of APC algorithm error was a last minute thermal blanketing modification to the antenna, made prior to launch but after the antenna range measurements were completed (Ruf ct. al, 1993b).

In-flight testing of the TMR calibration algorithms was carried out during the six month verification phase following launch. Various sources of "ground truth", including radiosondes, water vapor radiometers (WVRs), and climatological models, were compared with overflown TMR measurements in both the brightness temperature and retrieved path delay domains, Similar to verification studies for previously flown water vapor microwave sensors (Lipes, 1982; Alishouse et al., 1990), radiosondes were used as the primary calibration standard in the integrated water vapor (path delay) domain (Ruf et al., 1993b). Twenty-three island radiosonde launch sites, located within 50 km of the TOPEX/Poseidon ground track, were used as the comparison data base. Radiosondes offer t hrcc primary advantages for cal i brat ion of water v~por-related satellite measurements: no-cost availability, abundance of data, and direct measurement of the vapor and temperature profiles which determine the path delay. The primary disadvantages are large temporal and spatial decorrelations relative to the TMR measurements and errors in the radiosonde relative humidity measurements, c.specially in the presence of clouds or very dry conditions (Schwartz and Doswell, 1991). In addition, comparisons in the path delay domain alone do not reveal the source(s) of in-flight calibration errors. As demonstrated by the early TMR performance, and described in this paper, satisfactory comparisons can be obtained in the path delay domain while large, but compensating, errors arc present in the satellite brightness temperature measurements.

Ground-based WVRS arc especially useful for satellite microwave sensor calibration in the brightness temperature domain, WVRs directly measure the atmospheric emissions which arc the

main source of variability in the open ocean satellite microwave measurements. To predict TMR brightness temperatures from the WVR measurements, a sea sul-face flux model is required to account for the background contributions to the nadir-viewing measurements. For calm conditions this model is well constrained by knowledge of the sca surface temperature within an accuracy of a few degrees Kelvin. in fact, results of the final TMR algorithm adjustments suggest that the 'I'MI-t operational brightness temperature accuracies are sufficient to refine the calm ocean model flux levels at the TMR frequencies to accuracies of 1-2 K.

in this paper the role of WVRs in the TMR in-flight calibration is emphasized. In section 11 we describe the deployment and operational characteristics of the WVRS used in the TMR verification processing, Section II I presents results of 'I'MI{-WV]{ comparisons in the brightness temperature domain. 1)ata which led to the early detection of large TMR antenna calibration errors is shown, followed by the results of the first year of comparison data using the final TMR calibration algorithms. in this section evidence is presented suggesting that the actual calm sca flux is enhanced --2 K above the Fresnel predictions for a flat surface, Section I V presents "I'MR-WV]< comparisons in the path delay domain based on the final TMR algorithms and the first year of data, in section V the WVR comparison results arc summarized and lessons learned regarding the utilization of WVRS for satellite instrument calibration arc discussed.

II. WVR Deployment and Operation

For the purposes of validation of the altimeter and TMR performance, WVRs were deployed prior to cycle 1 measurements, and have continued operation, at 1.ampcdusa island (35.57N, 12.57E), in the Mediterranean Sea, and the 1 larvest oil platform (34.47N, 120.68 W), 11 km from the California coastline near Santa Barbara. These were the primary verification sites for the Poseidon (CNES) and TOPEX (NASA) altimeters respectively. The verification site WVRS arc identical three-frequency l-units, built at the Jet Propulsion Laboratory, with channels at 20.7, 22.'2, and 31.4 GHz (Keihm et al., 1993 b). in addition, a J]'], I)-unit WVR, operating, at 20.7 and 31.4 GHZ, was deployed for ~ one month periods at the island sites of Chichi lima, Japan (27.08N, 142. 18E) during September, 1992, and Norfolk, Australia (29.03S, 167.93E) from October 15-November 15, 1992. These sites were chosen for their proximity to the TOPEX/Poseidon groundtrack and to provide high (Chichi lima) and low (Norfolk) end humidity condition comparisons early in the verification phase, Minimum groundtrack separations at the four WVR silts arc 21 km at Lampedusa, () km at 1 larvest (direct overflight), 32 km at Chichi lima, and 29 km at Norfolk.

At all sites the WVRS operated in a continuous tipping, curve mode, monitoring instrument gain and zenith sky brightness temperature variations at a 1.5 minute sampling rate. In this mode absolute brightness temperature accuracies of 0.5 K have been demonstrated for the J and 1)-unit radiometers (Keihm, 1991). The zenith measurements were converted to integrated vapor abundance and path delay using statistical retrievals based on correlations with computed brightness temperatures from radiosonde data archives. The uncertainty in WVR-retrieved path delay is less than 0.3 cm duc 10

instrument effects alone. The largest error in the path delay retrieval is due to a ~ 5-1 00 / 0 uncertainty in the line strength of the vapor absorption model required to convert the measured brightness temperatures to vapor abundance (path delay). Since the same model of vapor absorption was used in both the TMR and WVR path delay retrieval algorithms, this error is transparent for '1 MR-WVR comparisons in the path delay domain,

In the brightness temperature domain, comparisons of TMR with WVR predictions required a conversion of the WVR measurements to the TMR frequencies and a model for the sea surface flux contribution to the (io\vr~\\'ard-\' it\\'it~~l, TMR. The frequency conversion produces negligible error because the vapor absorption model line shape is well constrained (1 lill, 1986; Keihm, 1992). For the sea surface flux component, measured sea surface temperatures were multi plied by temperature-dependent Fresnel emissivities calculated from the Klein and Swift (1977) formulation for ocean dielectric proper-tics. For the brightness temperature domain comparisons, only calm sea TMR data, as determined from the TMR wind speed algorithm (Keihm et al., 1993a), were used to minimize emissivity variations duc to wind-generated foam and roughness. The complete algorithm used to convert WVR brightness temperatures to predicted TMR brightness temperatures is presented by Ruf et al. (1993 b).

'through August, 1993, - 100 overflight comparisons of the WVR sites have been obtained, including twelve from the temporary stations at Chichi lima and Norfolk. At Lampedusa, where both ascending and descending ground tracks lie within 50 km of the site, 55 TMR-WVR comparisons were obtained over the first year of operation, No Lampedusa WVR data was obtained over a six week interval at the end of 1992 duc to a hardware failure incurred during, a severe electrical storm. At the Harvest oil platform numerous WVR hardware fail ures occurred, result ing in the loss of 12 of the first 40 cycles of overpass comparison data, These failures can be attributed to the harsh environmental conditions at Harvest. in addition to the salt sea air effects, the I larvest WVR is located less than four meters from a helicopter landing pad and is subject to intense vibrations four times daily during, the helicopter landings and takeoffs,

III. Results of TMR-WVR Brightness Temperature Comparisons

Early detection of 'I'M R bright ness temperature offsets

Within six weeks post-launch, prior to the completion of orbit maneuvers and the onset of cycle 1 data, 1 larvest and Lampedusa overflight comparisons of TMR and WVR-predicted brightness temperat urcs revealed 6-12 K offsets, with the 'I'M R low in all channels (Figure 1, open squares). The problem was not apparent in the path delay domain comparisons because the offsets produced largely compensating effects in the path delay retrieval algorithm. (Recall that the '1'Ml<-derived retrievals arc strongly correlated with the 21 minus 18 (i] lz brightness temperat urc differences.) To determine the source of the large offsets, a number of possible explanations were considered, including errors in the APC algorithm, errors in our assumed model of sca surface flux, and errors in the antenna temperature calibration, After eliminating the APC and surface flux model

uncertainties as insufficient to produce the observed offsets, we discovered that part of the pre-launch T/V data, used to calibrate the TMR sensitivity to the cold sky brightness temperature, was invalid due to large temperature gradients present in the T/V cold sky target. The error was corrected by identifying other 'T/V' data taken when the cold sky target temperature was stable. The resultant revised antenna temperature calibration algorithm essentially removed all of the biases relative to the WVR comparison data (cross data of Figure 1).

The results shown in Figure 1, based on the revised antenna temperature algorithm, do not represent the final TMR brightness temperature calibration. Smaller adjustments were later required based primarily on the TMR-radiosonde comparisons in the path delay domain. These comparisons revealed a scale error o - 10%, after the antenna temperature calibration revision, with the TMR-derived path delays increasingly low relative to the radiosondc measurements for moderate to high vapor conditions. The scale error was corrected by -- 5% refinements to both the APC algorithm and the vapor absorption model line strength used in the path delay retrieval algorithm, This division was based on a number of considerations. First, the "TMI<-WVI< path delay comparisons were consistent with a smaller scale error, -5%, although the number and range of the early comparisons were insufficient to constrain the scale error by better than a factor of two. This result suggested that al least part of the scale error was due to instrument calibration effects, since the TMR-WVR path delay comparisons arc transparent to absorption model errors. Second, comparisons of the TMR brightness temperatures with data from the Special Sensor Microwave/In~agcr (SSM/I) radiometer over the Amazon rain forest revealed biases of 6-9 K (TMR low) for the highest brightness temperatures measured, where gain errors have the largest effect. These high end offsets were corrected by gain adjustments in the APC algorithm of ~ 50/0 in the three TMR channels, performed in such a way as to correct -- half of the observed path delay scale error. The remaining scale error was eliminated by the So / O line strength reduction in the path delay retrieval algorithm's vapor absorption model. For a more detailed discussion of the final TMR algorithm modifications, scc Ruf et al. (1993b).

TMR-WVR brightness temperature comparisons using the final TMR calibration algorithms

The final TMR instrument gain adjustments have been used to recompute the TMR-measured versus WVR-predicted brightness temperature comparisons over the first full year of operation. The results, shown in figures 2-4 for the Harvest, Lampedusa, and Norfolk sites, include only overpasses characterized by low wind speeds and cloud free conditions. The Chichi Jima results arc not shown because only two of the overpasses satisfied the clear, calm criteria.

The figures clearly illustrate that the WVK predictions of TMR brightness temperatures arc systematically low for all three TMR channels. The larger offsets seen at 1 larvest and Lampedusa, relative to Norfolk, arc primarily duc to the effects of land mass contamination in the main beam (defined below) and side lobes of the TMR data at the primary verification sites. Norfolk Island is located -- 1 200 km from the eastern coast of Australia, with no closer large land masses. 'T'bus, no significant land enhancements in the TMR main beam or on-earth side lobes is expected for Norfolk overpasses. At 1 larvest, however, a significant fraction of the main beam and - half of the on-earth

side lobes view California and the western U.S. At Lampedusa, a smaller fraction of the main beam views Tunisia, but ~80% of the on-earth side lobes view the combined land masses of southern Europe, northern Africa, and southwestern Asia. This land contamination causes a significant enhancement in the measured TMR antenna temperatures. The brightness temperatures are similarly enhanced since the APC algorithm is designed for open ocean measurements.

To assess the land contamination effects at Harvest and Lampedusa, the pre-launch antenna pattern measurements were convolved with map-determined land mass fractions and the expected brightness temperature difference between land and water.

$$\Delta T_a \int_{0}^{\theta_1} P(\theta) \cdot f(\theta) \cdot \Delta T_b(\theta) \cdot d\theta \qquad (1)$$

where ΔT_a equals the antenna temperature enhancement relative to an open-ocean measurement, θ equals the polar angle measured from satellite nadir, $P(\theta) \cdot d\theta$ equals the fractional beam power in the annulus from θ to $\theta + d\theta$, $f(\theta)$ equals the land fraction at θ, and $\Delta T_b(\theta)$ equals the brightness temperature enhancement of land relative to water at θ. In Equation (1) a circular symmetric beam is assumed and $\theta_1 = 55°$ is the limit of the on-earth side lobes.

Similar to the APC algorithm (Janssen et al., 1993), the integral in Equation (1) can be divided into a main beam (θ 0-1 0) and the on-earth side lobes (0 10-55). Over the main beam equation (1) is solved numerically, dividing the integral into 100 increments of 0.1 degrees in θ, computing $f(\theta)$ from maps and the groundtrack coordinates at the point of comparison, and using a constant value of A "$T_b(0)$ equal to 260 minus the site overpass average TMR main beam brightness temperature, T_{avg}. (For all θ we assume a land brightness temperature of 260 K.) Over the on-earth side lobes (0 10-55), the differential beam power is slowly varying and the integral can be evaluated to sufficient accuracy by using averaged quantities, yielding

$$\int_{0}^{55} P(\theta) \cdot f(\theta) \cdot \Delta T_b(\theta) \cdot d\theta = b \cdot F_{10\text{-}55} \cdot (260 - T_c) \qquad (2)$$

where b equals the fractional beam power from θ 10-55, $F_{10\text{-}55}$ equals the [eta] land fraction from 0 10-5S, and T_c equals the latitude-dependent aver-age open-ocean on-earth brightness temper-aturc. Values of the above parameters used to compute land contamination effects at Harvest and Lampedusa are given in Table 1. Cumulative beam power fractions and land fractions in the main beam are shown in Figures 5 and 6. Note that the ground track position used for the Harvest comparisons is 40 km (θ ~ 1.7 degrees) from the coastline.

The computed results for the main beam, on-earth side lobe, and total land contamination effects at Harvest and Lampedusa are shown in Table 2. The largest effects are in the 18 and 21 GHz channels at Harvest for which the largest fraction of the main beam covers land. At Lampedusa,

1 ampedusa, which lies ~ 140 km from Tunisia, the perturbation is dominated by the on-earth side lobe effects and the fact that - 80% of the 10-55 degree beam views land,

The land-corrected TMR brightness temperature "offsets", relative to the WVR predictions al the overpass sites, are obtained by subtracting the total land effects in "1'able 2 from the measured offsets shown in figures 2 and 3. The results arc given in "1'able 3, including the Norfolk comparison data for which no land correction was applied. (Note that the relatively high beam efficiencies allow us to assume that the computed land effects are equivalent for antenna and brightness temperatures.) The important result is an apparent 1-2 K enhancement relative to the WVR predictions which can be attributed to a slightly higher calm sea surface flux than that predicted for a plane layer with the Klein-Swifl dielectric properties. Evidence exists that either small scale roughness (Gay danskiy et al,. 1988) or uncertainties in the Klein-Swift dielectric properly model above 10 GHz (Wentz, 1992) could account for the measured offsets,

The reliability of the 1-2 K enhancement result depends primarily on the uncertainties of the final TMR calibration algorithms. Based on an evaluation of the uncertainties of all constraints which determined the final calibration, an absolute TMR brightness temperature accuracy of 1.5 K is estimated (Ruf et al,, 1993b). The uncertainly of the Harvest and Lampedusa land contamination corrections is estimated to be < 20°A of the computed values based on uncertainties in the land fraction and land temperature estimates. The largest uncertainties arc for the 18 and 21 GHz channels at I larvest where the largest fractions of the main beam view land The reason why the highest residual offsets at all three TMR frequencies occur at the Lampedusa site is not clear. One possible explanation is an error in the on-earth side lobe fractions which would affect the Lampedusa land correction -- twice as strongly as at 1 larvest. It is noteworthy that the results from Norfolk island, where land contamination effects arc negligible, support a 2 K enhancement.

IV. Results of TM R-WVR Path Delay Comparisons

The first full year of TMR-WVR overpass path delay retrieval comparisons are shown in Figures 7 (Harvest), 8 (Lampedusa), and 9 (Norfolk and Chichi lima), The final TMR calibration algorithms have been used, and the WV}{ retrieval algorithms have been modified to reflect the 5% decrease in the vapor absorption model line strength incorporated into the TMR algorithm, With the exception of two unexplained outliers at Harvest, all data is shown, including, high wind and cloudy cases. Most of the biases seen at Harvest and Lampedusa can be explained by the land contaminant ion effects, which have not been removed from the TMR data for these comparisons. "1 'he largest bias, - 1 cm at Lampedusa, is consistent with the 0.9 K relative offset (Figures 3a, 3b) between the 21 and 18 GHz channels at Lampedusa. It is noteworthy that, when the land contamination corrections arc applied at Harvest and Lampedusa, the rms residuals at all sites arc less than 1 cm of path delay difference, well within the mission specification accuracy of 1.2 cm.

The scatter at all sites is remarkably low, especially when the effects of WVR and spatial decorrelation errors arc taken into account. This result illustrates an important advantage of

utilizing WVRS for the in-flight calibration of vapor sensing radiometers. An island-deployed WVR, located on or near the satellite groundtrack, eliminates almost all of the decorrelation errors inherent to radiosor]dc-satellite comparisons. By contrast, the TMR-radiosonde path delay comparisons, used to fine tune the final TMR algorithms, were characterized by rms residual differences of ~3 cm, almost all of which could be attributed to spatial and temporal decorrelations between the vapor burdens sensed by the TMR and radiosondes (Ruf et al., 1993b).

The mean slope of the scatter plot for Lampedusa (Figure 8), suggests the presence of a small residual scale error in the final TMR algorithm path delay retrievals, A similar finding has been reported based on global TMR comparisons with the European Center for Medium range Weather Forecasting (ECMWF) climatological model (Stum, 1993). The ECMWF model, based largely on the global interpolation of surface and radiosonde data, successfully predicts global-scale features of the path delay variations, but often produces 100-500 km errors in the positioning of sharp latitude-dependent features (Stum, 1993), In contrast, the final-algorithm TMR comparisons with individual near-gmundtrack radiosonde measurements yield no scale error in the path delay domain (Ruf et al., 1993b). The zero scale error result is also supported by comparisons oi'the TMR and ERS-1 satellite radiometer path delay retrievals in the vicinity of crossover points (Stum, 1993). Based on the results of the more direct comparisons, we believe that the apparent scale error seen in the Lampedusa TMR-WVR path delay comparisons is most likely due to a small residual "gain" error associated with the uncertainties of the land contamination effect.

V. Summary and Discussion

Ground-based water vapor radiometers provided valuable comparison data for the in-flight calibration and performance assessment of the 'TOPEX Microwave Radiometer-. WVR-based predictions of TMR brightness temperatures at the Harvest and Lampedusa verification sites provided early recognition of large TMR offsets and constrained the resultant antenna temperature calibration algorithm correction. Later TMR-WVR comparisons, using the final TMR calibration algorithms and the first year of calm sea data, demonstrated the importance of land contamination effects at the Harvest and Lampedusa verification sites. After application of corrections for the land effects, the TMR vs. WVR-predicted brightness temperature comparisons indicated average offsets of 1-2. K (TMR high), indicative of a correction to be applied to the Fresnel model of the cairn sea surface emissivity.

Comparisons of TMR and WVR path delay retrievals at four ground sites demonstrated the importance of co-location and time synchronization for water vapor-related data, Spatial and temporal decor-relations inherent to the traditional radiosonde site path delay comparisons produce ~3 cm of rms residual for average space and time separations of 100 km and 3 hours (Ruf et al., 1993b). Uncertainties in the evaluation of the decorrelation contribution to the large radiosonde comparison scatter makes it difficult to assess the satellite radiometer path delay performance at the 1 cm level. In contrast, the time-synchronized and nearly co-located WVR-? data yielded TMR comparison residuals < 1cm after land contamination corrections were applied.

We are not suggesting that WVRs should replace radiosondes as the primary ground truth data base for in flight calibration of satellite radiometers. in many ways, the WVR and radiosonde data are complimentary. The radiosonde stations rapidly provide a large global data base which const[-sins biases and scale errors in the water vapor-related satellite radiometer retrievals. For vapor-induced path delay, the radiosonde measurements are direct, not requiring a model-cicpcndcnt conversion from measured brightness temperatures. WVRs are most useful for the satellite radiometer brightness temperature calibration and instrument performance monitoring. The direct measurement of sk?'brightness temperatures at or near the satellite radiometer frequencies provides an accurate (0.5K) constraint on the highly variable atmospheric contributions to the downward-viewing instrument. The addition of a well-cmstraincd calm sca surface flux component to the WVR measurements then allows direct comparisons in the brightness temperature domain, yielding satellite radiometer calibration accuracies at the 1 K level.

For future altimetry satellite missions which include a microwave radiometer to provide the tropospheric range correction, it is recommended hat one WVR be included to supplement the standard global radiosonde comparisons in the in-flight verification plan. The ideal deployment location would be a small island radiosonde station, at least 500 km from the nearest large land mass, and within 50 km of a mid-latitude node crossing position of the satellite ground track. As demonstrated by the WVR performance at 1 ampedusa, the instrument could operate in an unattended mode for a year or more, with data transfer via modem or monthly downloading by radiosondc station personnel. The required on-site manpower support is minimal, consisting mainly of prc-overflight checks which include cleaning of the WVR radomc and reflector surfaces. 1 Deployment at a radiosondc weather station would also provide useful support data such as cloud cover, wind speed, and comparisons to monitor the WVR performance.

other desirable characteristics of the deployment site would include a high percentage of low wind and cloud-free conditions and large seasonal variations in vapor abundance. Calm and clear conditions minimize comparison uncertainties associated with wind-induced emissivity variations and horizontal variations in the cloud effects, The seasonal variations determine the dynamic range over which the instrument calibration and retrieval performance can be monitored, Radiosonde data statistics from candidate island weather stations would be analyzed to find a site which best satisfies the above criteria,

ACKNOWLEDGMENTS

The authors would like to acknowledge several individuals and organizations for their assistance with this work. Peter Gaiser and Karen St, Germaine of the University of Massachusetts deployed and operated the WVRS at Chichi Jima and Not-folk. The Japanese Local Meteorological observatories and the Australian Bureau of Meteorology were very helpful in facilitating the WVR deployments at Chichi Jima and Norfolk. Robert Jablonski and Philip de Blieck, under the authority of Commander LTJG Catalano at the U.S. Coast Guard station at Lampedusa, monitored the performance of the Lampedusa WVR and provided timely data transfers throughout the first year

of operation. Alan Tanner of the Jet Propulsion Laboratory maintained the WVRs at Harvest and Lampedusa.

This work presents the results of one phase of research conducted at the Jet Propulsion Laboratory, (California Institute of Technology, Pasadena, CA, under contract to the National Aeronautics and Space Administration.

REFERENCES

Alishouse, J.C., S.A. Snyder, J. Vongsathorn, and R.R. Ferraro. 1990. Determination of oceanic total precipitable water from the SSM/I, *IEEE Trans. Geosci. Rem. Sensing*, 28:811-816.

Carlisle, G., A. Dicicco, H.M. Harris, A. Salama, and M. Vincent. 1991. TOPEX/POSEIDON *Project Mission Plan*, Jet Propulsion Laboratory, Pasadena, CA, Document No. D-6862, Rev. B.

Gaydanskiy, S.I., V.Y. Gershenzon, and V.K. Gromov. 1988. Detection of surface manifestations of internal waves in the ocean by microwave radiometry, *Izvestiya, Atmos. Ocean. Physics*, 24:731-735.

Hill, R.J. 1986. Water vapor-absorption line shape comparison using the 22-GHz line: The Van Vleck-Weisskopf shape affirmed, *Rad. Sci.*, *21:447-451.*

Janssen, M.A., C.S. Ruf, and S.J. Keihm. 1993. TOPEX/POSEIDON Microwave Radiometer (TMR): I, Antenna pattern correction and brightness temperature algorithm, submitted for publication in *IEEE Trans. Geosci. Rem. Sensing.*

Keihm, S.J. 1991, Water vapor radiometer intercomparison experiment: Platteville, Colorado, March 1-14, 1991. Final report prepared for Battelle, Pacific Northwest Laboratories on behalf of the Department of Energy. Jet Propulsion Laboratory Doc. No. D-8898.

Keihm, S.J. 1992. Atmospheric absorption from 20-32 GHz: Radiometric constraints on the vapor and oxygen components. *Proc. of Specialists Meeting on Microwave Radiometry and Remote Sensing Applications*, E.R. Westwater, ed., Boulder, Colorado, 211-218.

Keihm, S.J., M.A. Janssen, and C.S. Ruf. 1993. TOPEX/POSEIDON Microwave Radiometer (TMR): III. Wet troposphere range correction algorithm and pre-launch error budget. Submitted for publication in *IEEE Trans. Geosci. Rem. Sensing.*

Keihm, S.J., N. Yamane, A. Tanner, R. Swindlehurst, S. Walter, and R. Newsted. 1993. Water vapor

radiometer measurements at Harvest Platform. in NASA Verification Site Report: Cycles 1-30. Jet Propulsion Laboratory 1 Doc. No. 1 D-xxxx.

Klein, L.A. and C.T. Swift. 1977. An improved model for the dielectric constant of sca water at microwave frequencies. /11/;/1,/. *Oceanic Eng.* OI ;-2:1 04-111.

Lipes, R.G. 1982.1 Description of S1 ASAT Radiometer status and results. *J. Geophys. Res.* 87:3385-3395,

Ruf, C.S., Keihm, S.J., and M.A. Janssen. 1993a. TOPEX/POSEIDON Microwave Radiometer. (I'MI<): I. Instrument description and antenna temperature calibration Submitted for publication in *IEEE Trans. Geosci. Rem. Sensing.*

Ruf, C.S., S.J. Keihm, B. Subramanya, M.A. Janssen, and '1'. I Liu. 1993b. TOPEX/POSEIDON Microwave Radiometer performance and in-night calibration. Submitted for publication in *J. Geophys. Res.-Oceans TOPEX Poseidon Special Issue.*

Schwartz, B. I{. and C.A. Doswell 1 II. 1991. North American rawinsonde observat ions: Problems, concerns. and a call to action. *Bull. Amer. Meteorol. Soc.* 72:1885-1896.

St um, J. 1993. A comparison between '1'01'11X Microwave Radiometer, I ERS-1 Microwave Radiometer and ECMWF derived wet tropospheric corrections, Submitted for publication in *J. Geophys. Res.-Oceans TOPEX Poseidon Special Issue.*

Wentz, F.J. 1992. Measurement of oceanic wind vector using satellite microwave radiometers. *IEEE Trans. Geosci. Rem. Sensing* 30:960-972.

Table 1. Parameter Values Used to Compute Land Contamination Effects at Harvest and Lampedusa

Parameter	Harvest	Lampedusa
b(18): 18 GHz On-Earth Beam Fraction	0.0278	0.0278
b(21): 21 GHz On-Earth Beam Fraction	0.0247	0.0247
b(37): 37 GHz On-Earth Beam Fraction	0.0?1s	0.0215
T_e(18): 18 GHz open-ocean On-Earth T_b (K)	170	170
T_e(21): 21GHz open-ocean On-Earth T_b (K)	170	170
T_e(37): 37GHz open-ocean On-Earth T_b (K)	169	169
T_{avg}(18): 18GHz Average Main Beam T_b (K)	127	130
T_{avg}(21): 21 GHz Average Main Beam T_b (K)	146	150
T_{avg}(37): 37 GHz Average Main Beam T_b (K)	156	156
$F_{10\text{-}55}$: Land Fraction, On-Earth Side Lobes	0.48	0.80

Table 2. TMR Land Contamination Effects on TMR Brightness Temperatures at Harvest and Lampedusa

	--------Harvest--------			-------Lampe -------		
TMR Channel	Main Beam	On-earth side lobes	Total	Main Beam	On-earth side lobes	Total
18 GHz	2.5 K	1.2 K	3.7 K	0.2 K	2.0 K	2.2 K
21 GHz	1.8	1.1	2.9	0.2	1.8	2.0
37 GHz	0.8	0.9	1.7	0.2	1.5	1.7

Table 3. Net Brightness Temperature offsets: Corrected TMR minus WVR-predicted

TMR Channel	Harvest	Lampedusa	Norfolk
18 GHz	0.2 K	1.9 K	1.4 K
21 GHz	1.1	3.0	1.4
37 GHz	1.7	2.1	1.9

FIGURE CAPTIONS

Figure 1. Pre-cycle 1 comparisons of measured and WVR-predicted TMR brightness temperatures at the 1 larvest and Lampedusa verification sites. The 6-12 K TMR offsets were effectively removed when post-launch corrections to the antenna temperature calibration algorithm were applied. The final modifications to the TMR antenna pattern algorithm have not yet been implemented.

Figure 2. Harvest overpass comparisons of measured and WVR-predicted TMR brightness temperatures for clear, calm conditions through cycle 40. The final TMR calibration algorithms have been utilized, but no corrections for land contamination have been applied.

Figure 3. Same as Figure 2, but for Lampedusa overpass data.

Figure 4. Same as Figure 2, but for Norfolk overpass data.

Figure 5. Cumulative TMR beam power as a function of polar angle as determined from pre-launch antenna pattern measurements. Within the main beam (0 0-10 degrees), each degree of polar angle corresponds to -23.3 km along the earth's surface.

Figure 6. Land fractions within the TMR main beam vs. polar angle at the Harvest and Lampedusa verification sites. At Harvest the TMR groundtrack location for comparisons with the WVR data is chosen to be 40 km from the California coastline (- 30 km from the 1 larvest platform),

Figure 7. Harvest overpass comparisons of TMR-retrieved and WVR-retrieved path delay for data through cycle 40, including cloudy and windy cases, The final TMR calibration algorithms have been utilized, but no land correction applied.

Figure 8. Same as Figure 7, but for Lampedusa overpass data, The much greater number of comparison data (relative to 1 larvest) is duc to the occurrence of two near overpasses for each cycle at the node-crossing Lampedusa site,

Figure 9. Same as Figure 7, but for the Norfolk and Chichi Jima overpass data. Only two of the four Chichi Jima overpasses arc included due to the occurrence of rain during two of the overpasses.

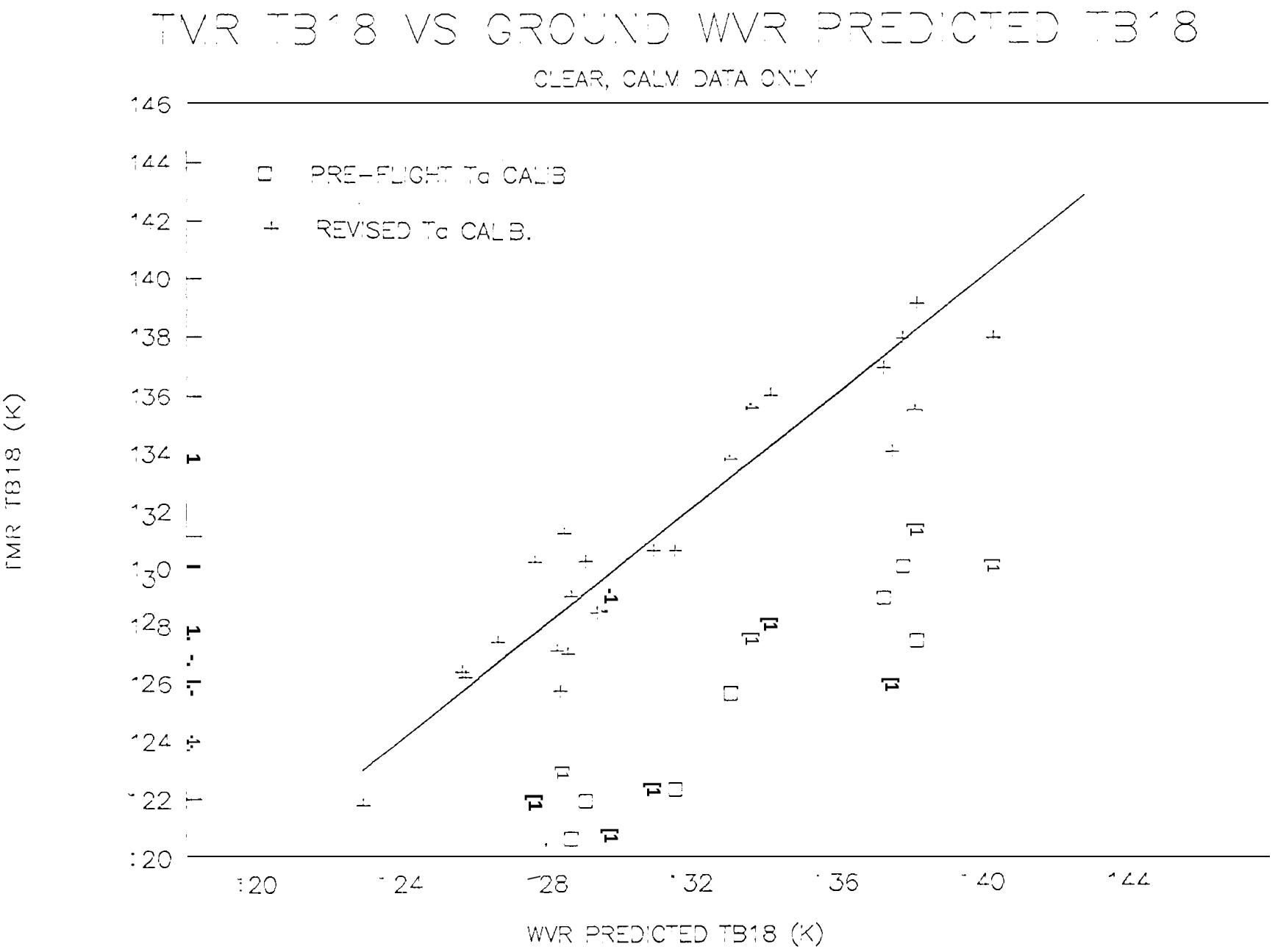
TVR TB18 VS GROUND WVR PREDICTED TB18
CLEAR, CALM DATA ONLY
PRE-FLIGHT To CALIB
REVISED To CALIB.
TMR TB18 (K)
WVR PREDICTED TB18 (K)
146
144
142
140
138
136
134
132
130
128
126
124
122
120
120
124
128
132
136
140
144

Fig. 12

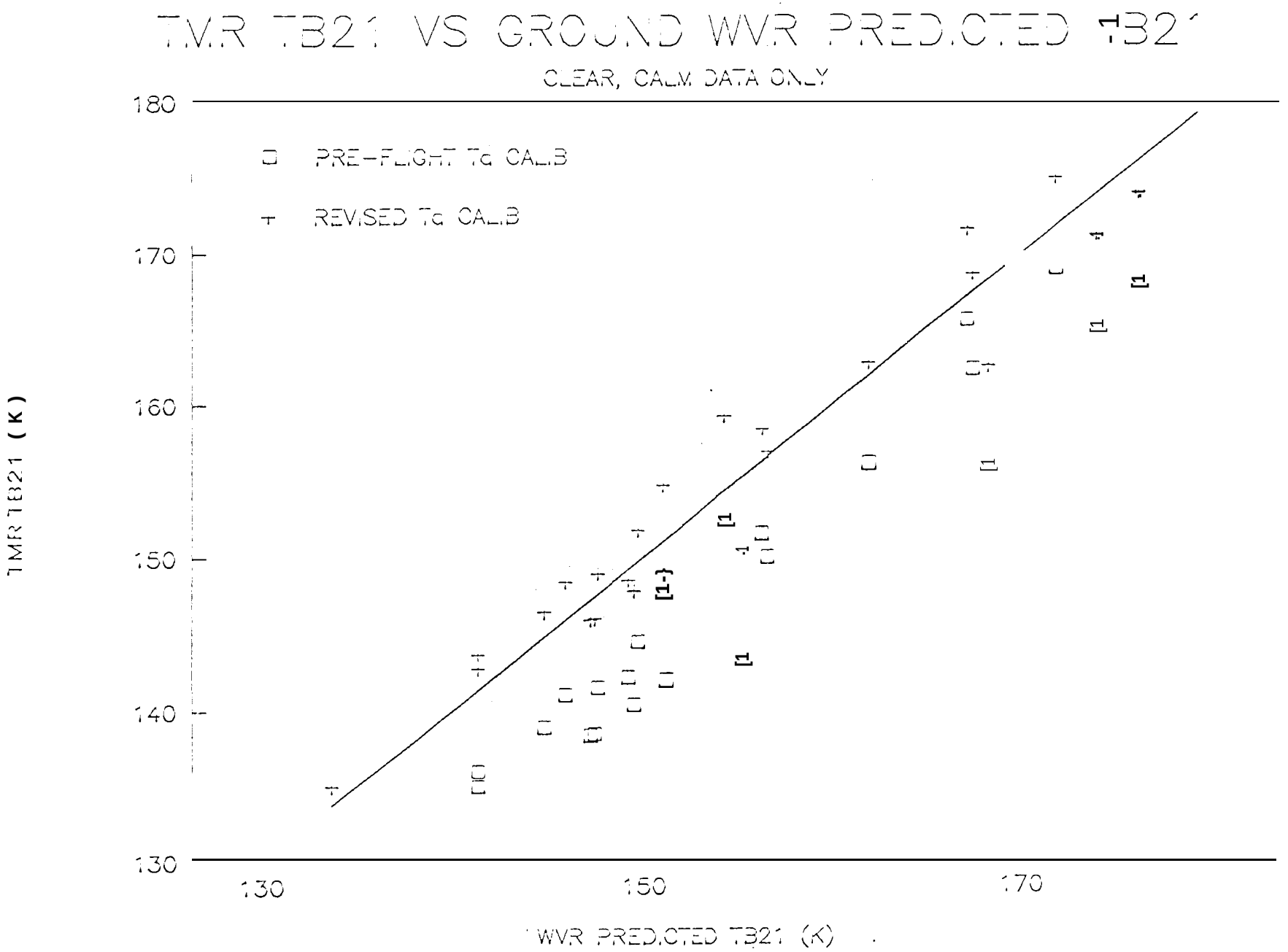
T.M.R TB21 VS GROUND WVR PREDICTED TB21
CLEAR, CALM DATA ONLY
PRE-FLIGHT Tc CALIB
REVISED Tc CALIB
TMR TB21 (K)
WVR PREDICTED TB21 (K)
180
170
160
150
140
130
130
150
170

TMR TB37 (K)

Fig. 1

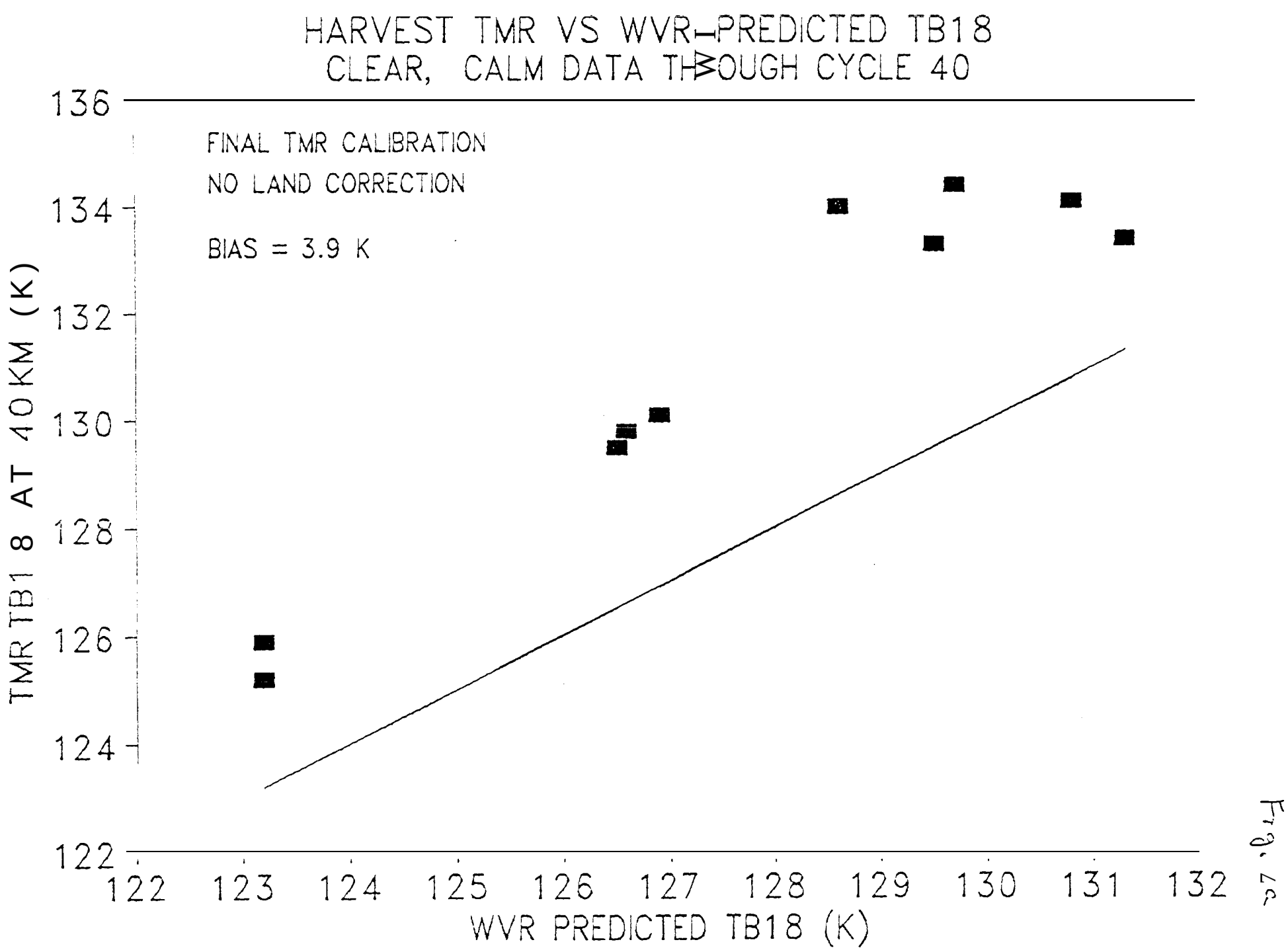
HARVEST TMR VS WVR-PREDICTED TB18
CLEAR, CALM DATA THROUGH CYCLE 40
FINAL TMR CALIBRATION
NO LAND CORRECTION
BIAS = 3.9 K
TMR TB18 AT 40 KM (K)
136
134
132
130
128
126
124
122
122
123
124
125
126
127
128
129
130
131
132
WVR PREDICTED TB18 (K)

Fig. 4c

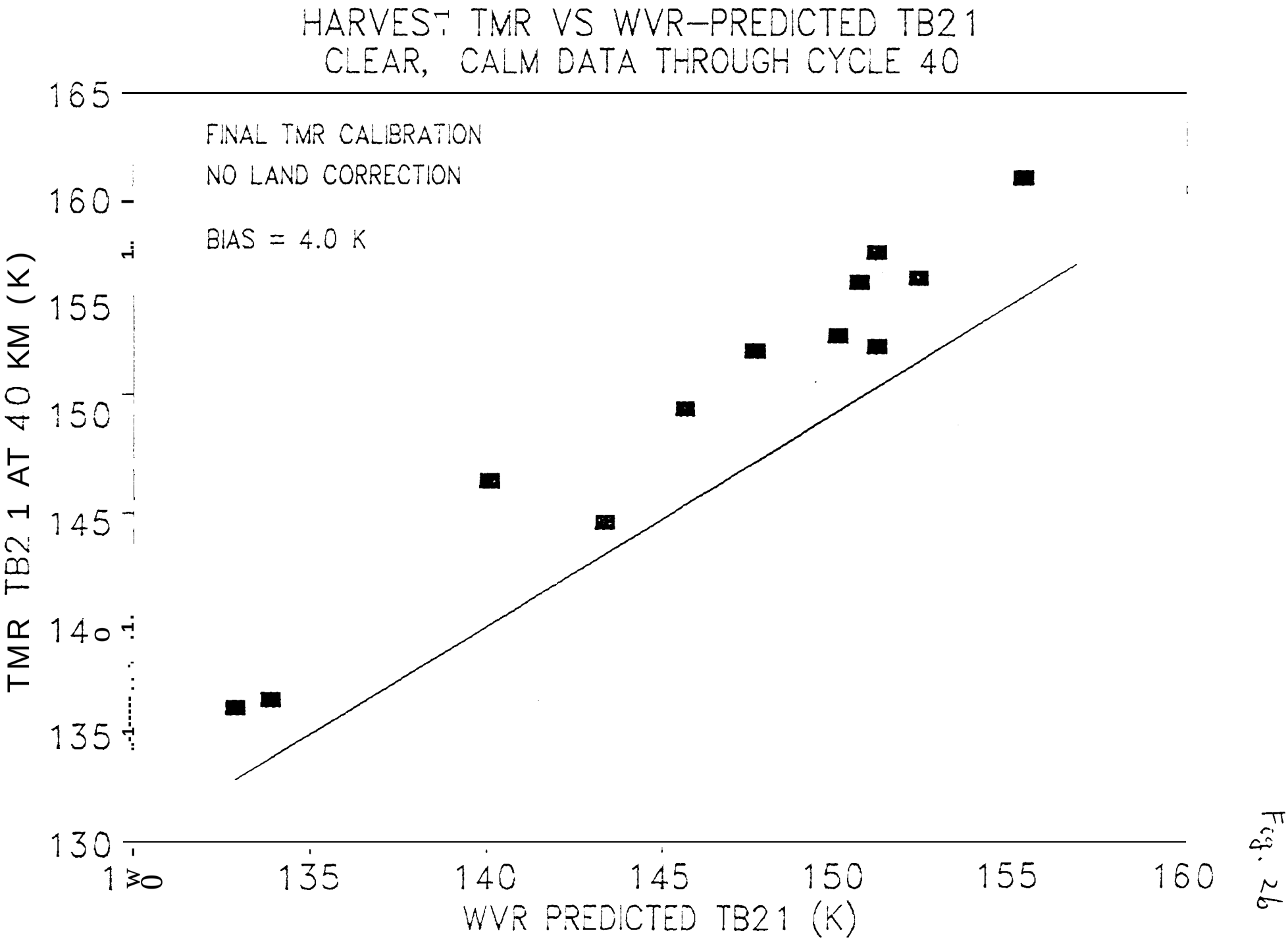
HARVEST TMR VS WVR–PREDICTED TB21
CLEAR, CALM DATA THROUGH CYCLE 40
FINAL TMR CALIBRATION
NO LAND CORRECTION
BIAS = 4.0 K
TMR TB21 AT 40 KM (K)
WVR PREDICTED TB21 (K)
165
160
155
150
145
140
135
130
135
140
145
150
155
160

Fig. 26

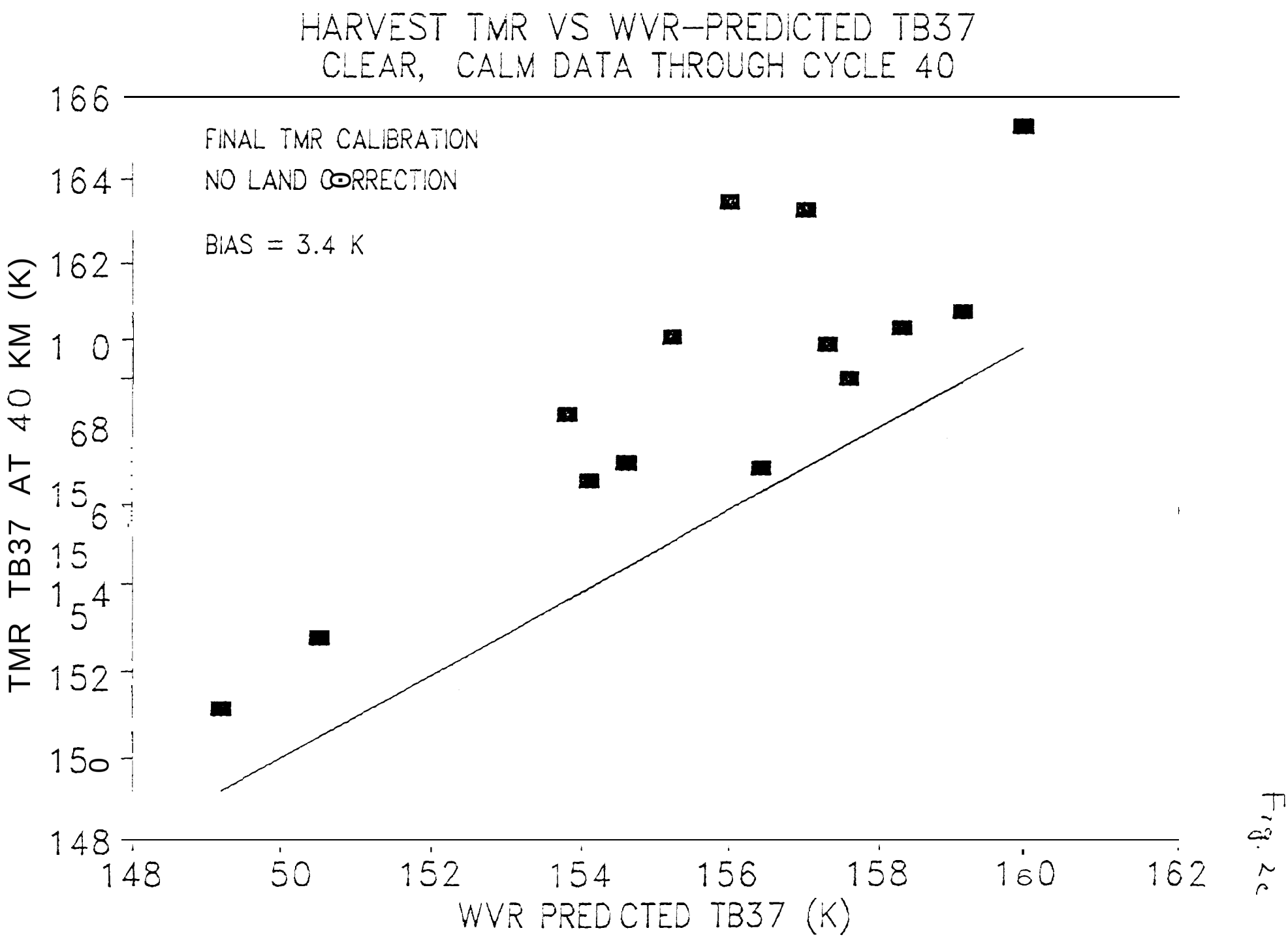
HARVEST TMR VS WVR–PREDICTED TB37
CLEAR, CALM DATA THROUGH CYCLE 40
FINAL TMR CALIBRATION
NO LAND CORRECTION
BIAS = 3.4 K
TMR TB37 AT 40 KM (K)
WVR PREDICTED TB37 (K)
166
164
162
160
158
156
154
152
150
148
148
150
152
154
156
158
160
162

Fig. 2c

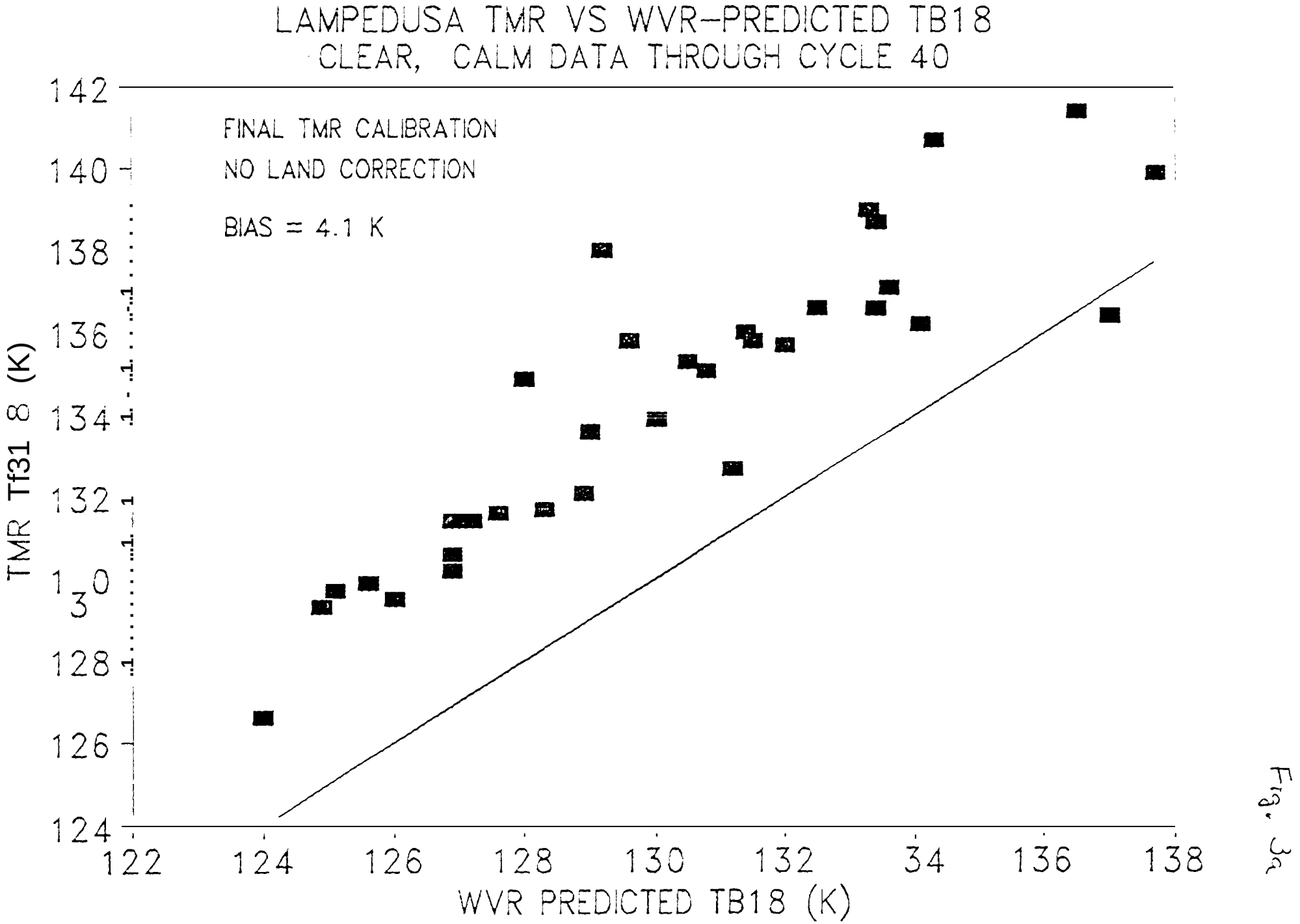
LAMPEDUSA TMR VS WVR-PREDICTED TB18
CLEAR, CALM DATA THROUGH CYCLE 40
FINAL TMR CALIBRATION
NO LAND CORRECTION
BIAS = 4.1 K
TMR Tf31 8 (K)
WVR PREDICTED TB18 (K)
142
140
138
136
134
132
130
128
126
124
122
124
126
128
130
132
34
136
138

Fig. 3c

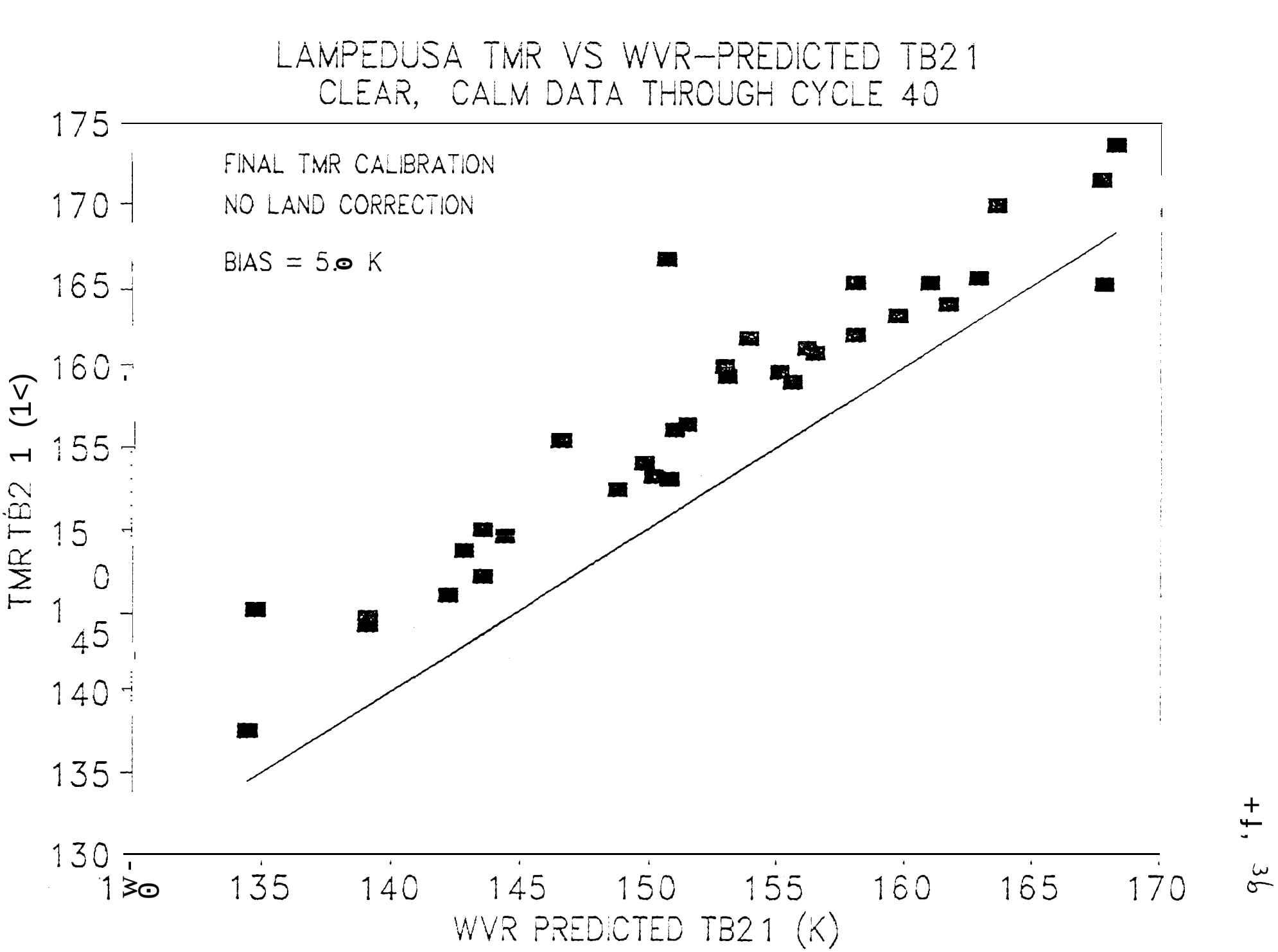
LAMPEDUSA TMR VS WVR-PREDICTED TB21
CLEAR, CALM DATA THROUGH CYCLE 40
FINAL TMR CALIBRATION
NO LAND CORRECTION
BIAS = 5.0 K
TMR TB2 1 (1<)
WVR PREDICTED TB21 (K)
175
170
165
160
155
150
145
140
135
130
135
140
145
150
155
160
165
170

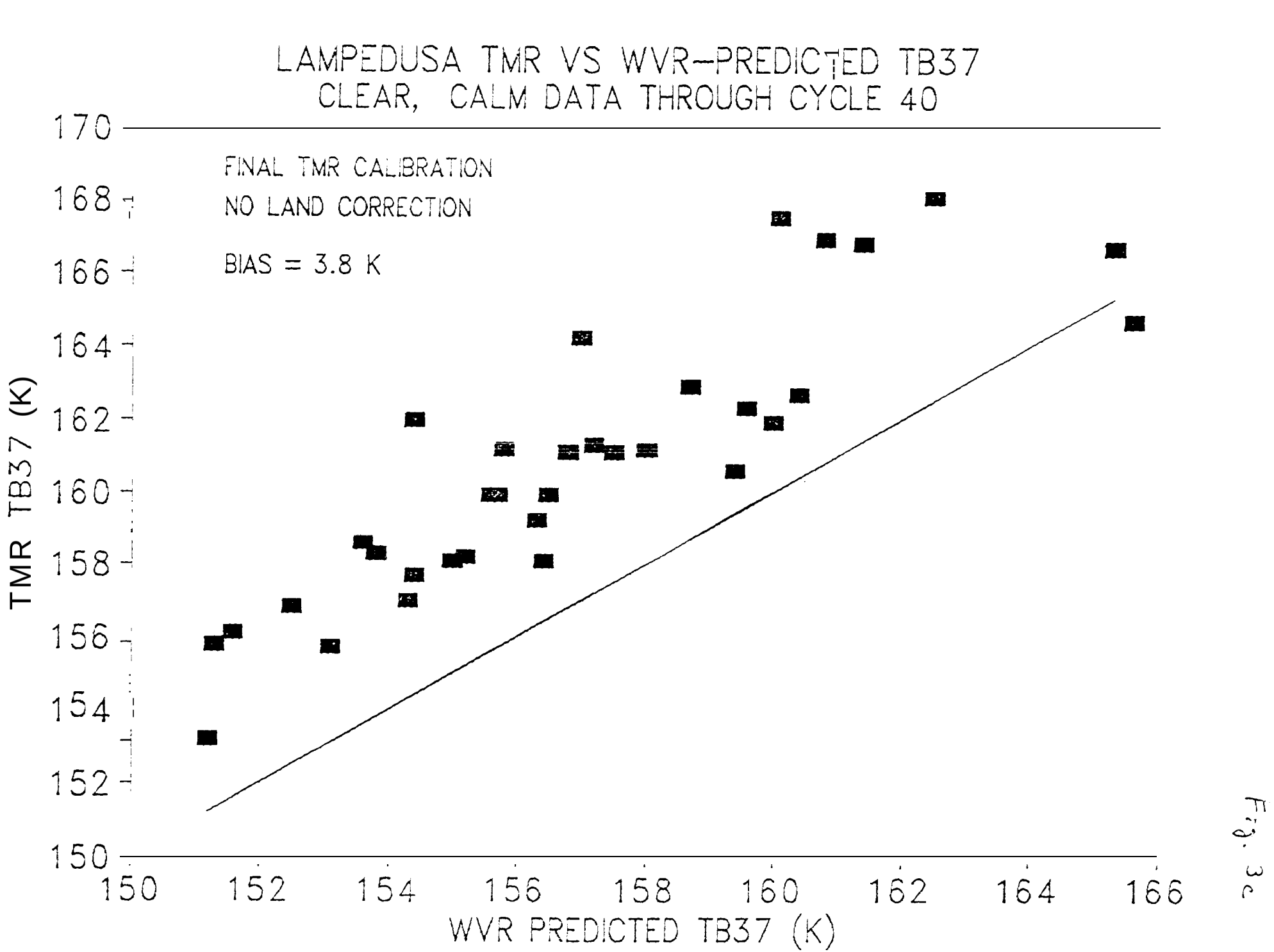
LAMPEDUSA TMR VS WVR-PREDICTED TB37
CLEAR, CALM DATA THROUGH CYCLE 40
FINAL TMR CALIBRATION
NO LAND CORRECTION
BIAS = 3.8 K
TMR TB37 (K)
WVR PREDICTED TB37 (K)
150
152
154
156
158
160
162
164
166
168
170

Fig. 3c

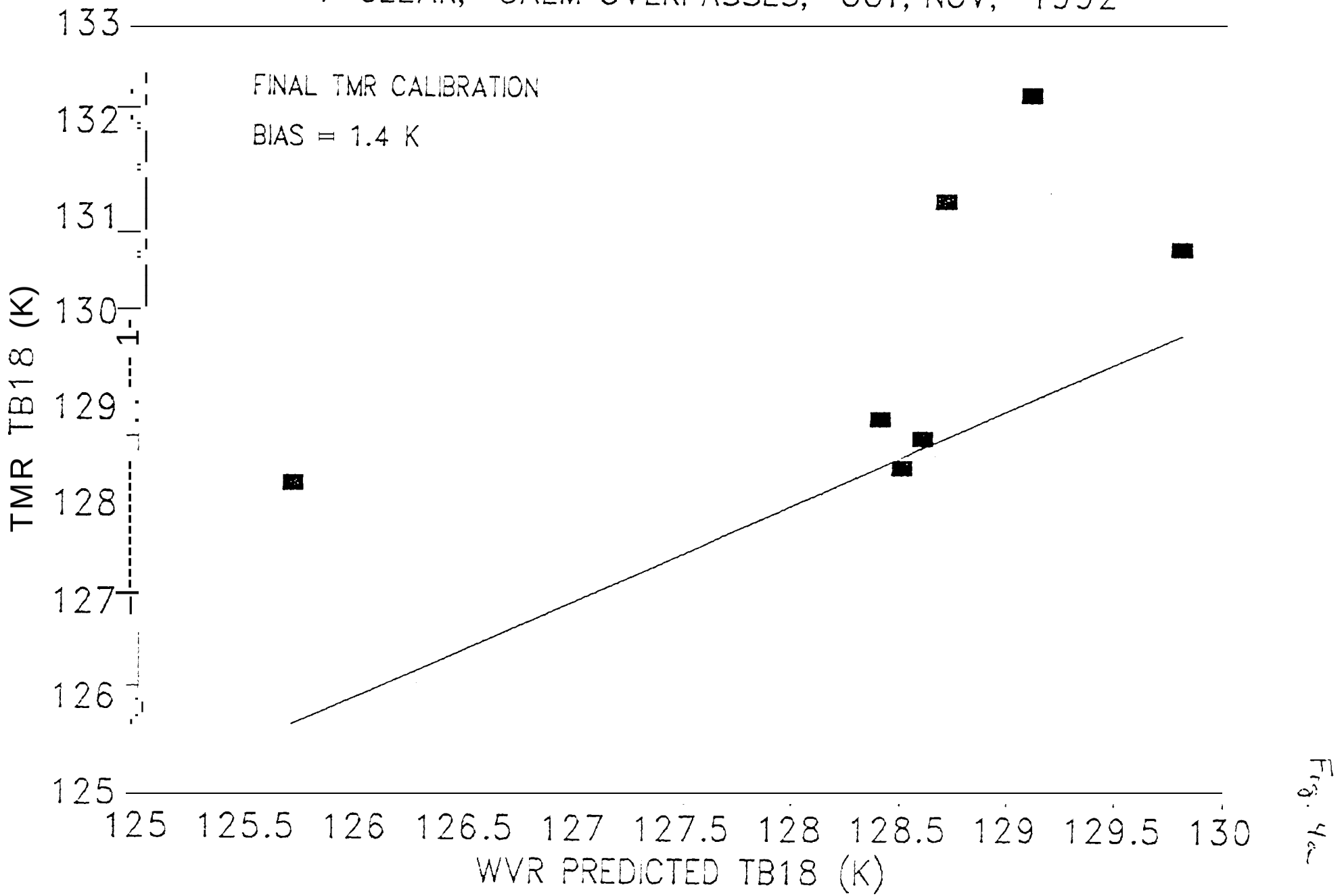
NORFOLK TMR VS WVR–PREDICTED TB18
7 CLEAR, CALM OVERPASSES, OCT, NOV, 1992
FINAL TMR CALIBRATION
BIAS = 1.4 K
TMR TB18 (K)
133
132
131
130
129
128
127
126
125
125 125.5 126 126.5 127 127.5 128 128.5 129 129.5 130
WVR PREDICTED TB18 (K)

Fig. 4a

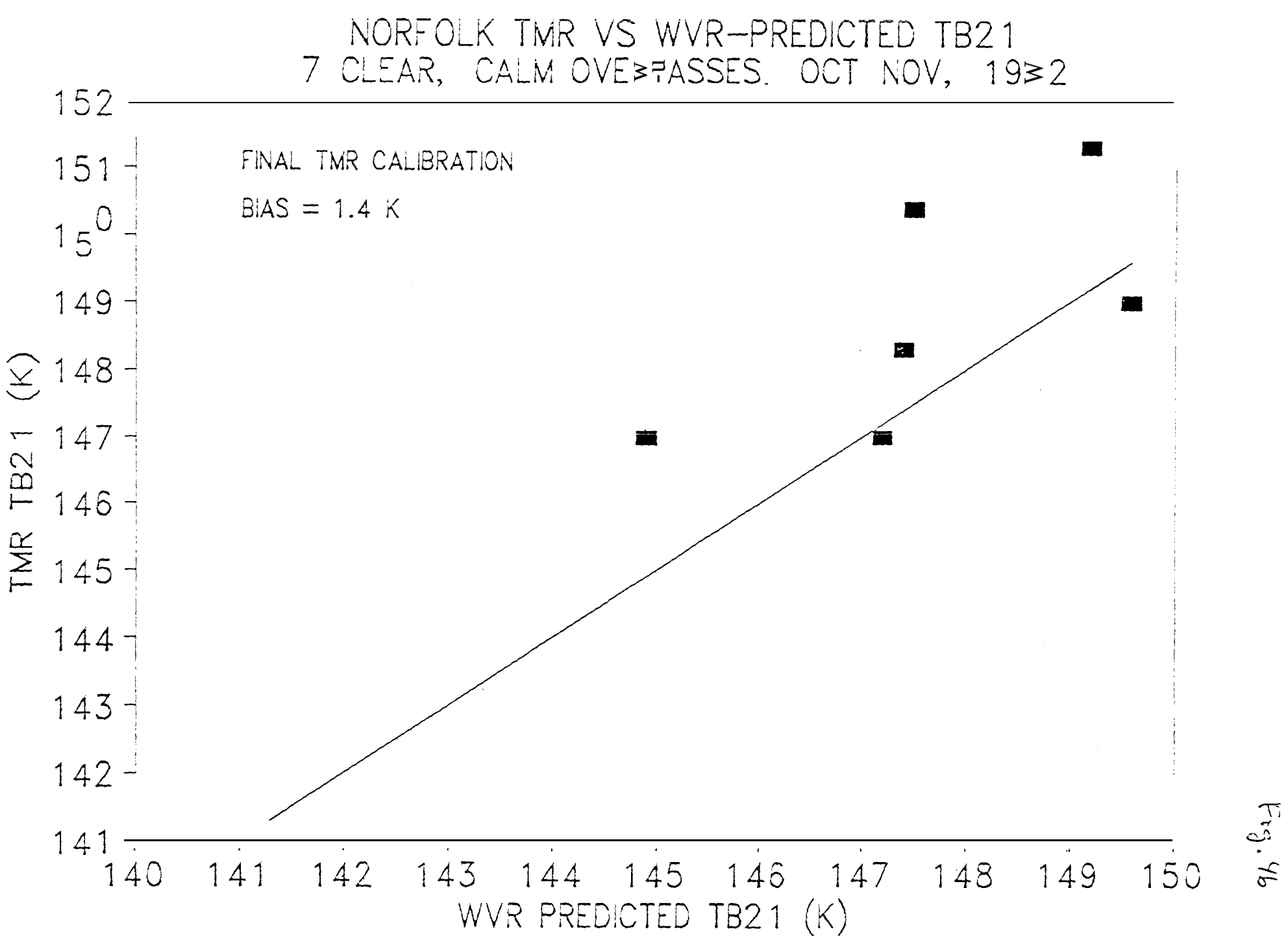
NORFOLK TMR VS WVR-PREDICTED TB21
7 CLEAR, CALM OVERPASSES. OCT NOV, 1992
FINAL TMR CALIBRATION
BIAS = 1.4 K
TMR TB21 (K)
WVR PREDICTED TB21 (K)
152
151
150
149
148
147
146
145
144
143
142
141
140
141
142
143
144
145
146
147
148
149
150

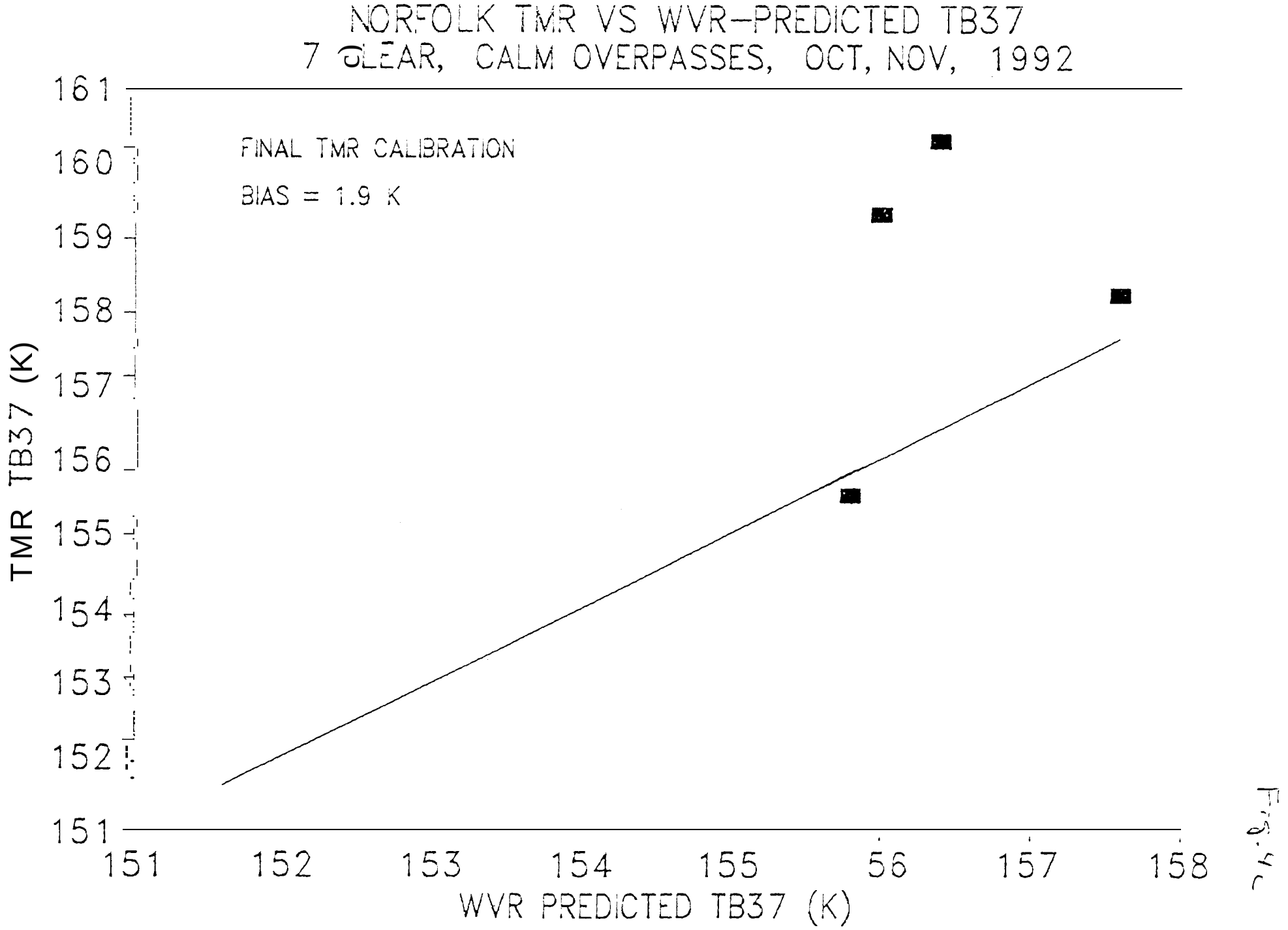
NORFOLK TMR VS WVR-PREDICTED TB37
7 CLEAR, CALM OVERPASSES, OCT, NOV, 1992
FINAL TMR CALIBRATION
BIAS = 1.9 K
TMR TB37 (K)
WVR PREDICTED TB37 (K)
161
160
159
158
157
156
155
154
153
152
151
151
152
153
154
155
56
157
158

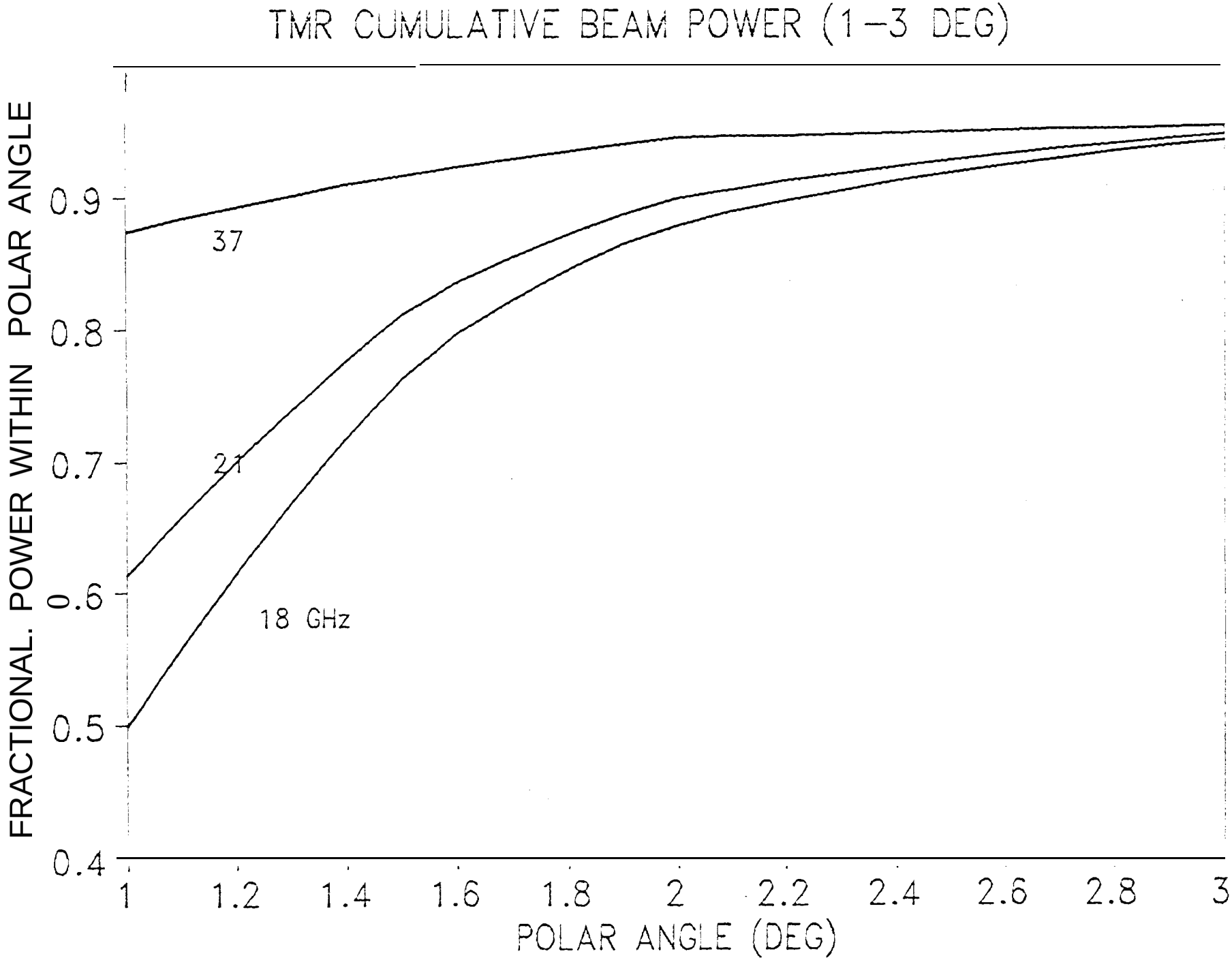
TMR CUMULATIVE BEAM POWER (1–3 DEG)
FRACTIONAL. POWER WITHIN POLAR ANGLE
0.9
0.8
0.7
0.6
0.5
0.4
37
21
18 GHz
1
1.2
1.4
1.6
1.8
2
2.2
2.4
2.6
2.8
3
POLAR ANGLE (DEG)

Fig. 5

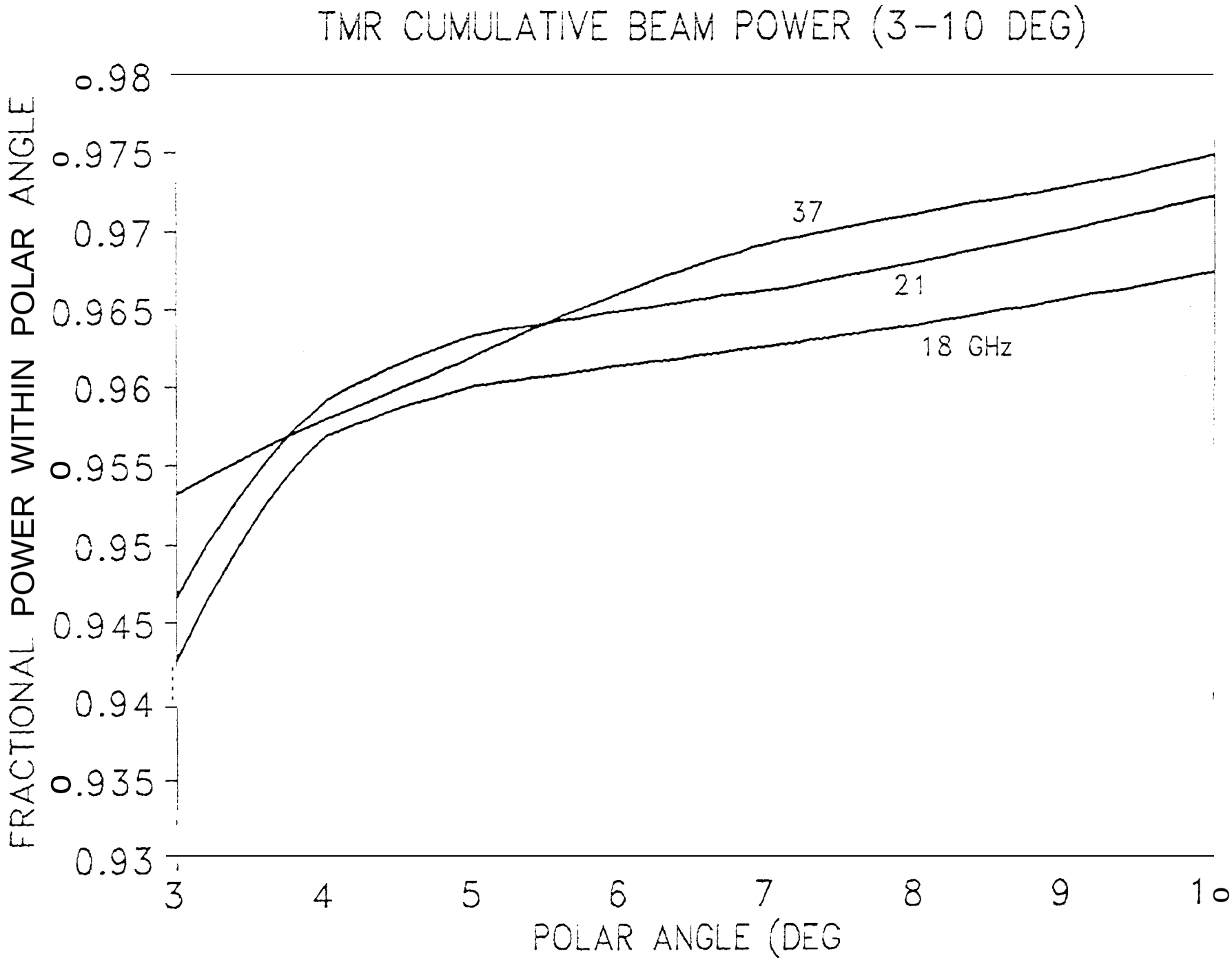
TMR CUMULATIVE BEAM POWER (3-10 DEG)
FRACTIONAL POWER WITHIN POLAR ANGLE
0.98
0.975
0.97
0.965
0.96
0.955
0.95
0.945
0.94
0.935
0.93
37
21
18 GHz
3
4
5
6
7
8
9
10
POLAR ANGLE (DEG

Fig. 6.3

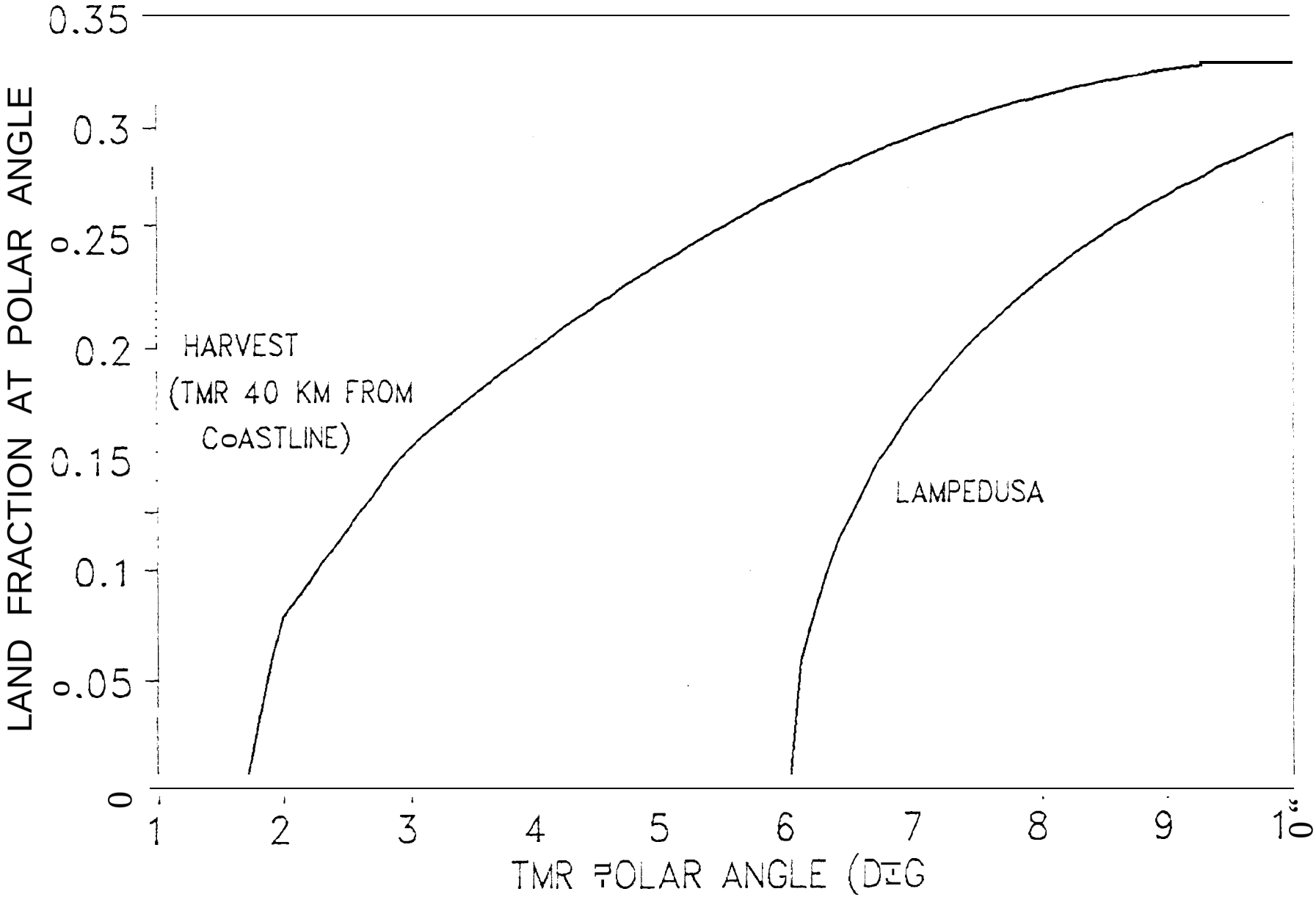
TMR LAND FRACTIONS VS. POLAR ANGLE
HARVEST, LAMPEDUSA VERIFICATION SITES
LAND FRACTION AT POLAR ANGLE
0.35
0.3
0.25
0.2
0.15
0.1
0.05
0
HARVEST
(TMR 40 KM FROM
COASTLINE)
LAMPEDUSA
1
2
3
4
5
6
7
8
9
10
TMR POLAR ANGLE (DEG

Fig. 6b

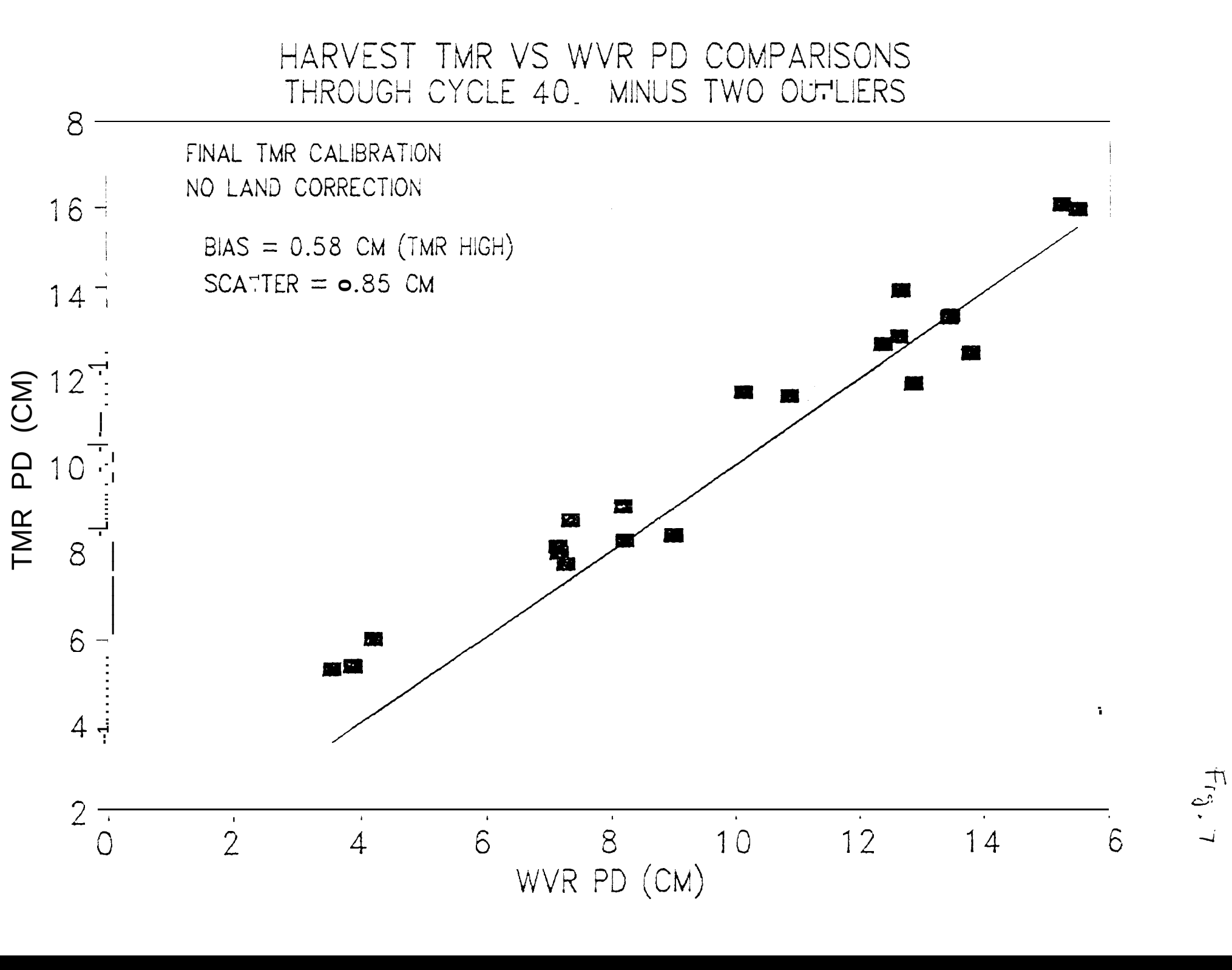
HARVEST TMR VS WVR PD COMPARISONS
THROUGH CYCLE 40. MINUS TWO OUTLIERS
FINAL TMR CALIBRATION
NO LAND CORRECTION
BIAS = 0.58 CM (TMR HIGH)
SCATTER = 0.85 CM
TMR PD (CM)
WVR PD (CM)
2
4
6
8
10
12
14
16
0
2
4
6
8
10
12
14
16

Fig. 7

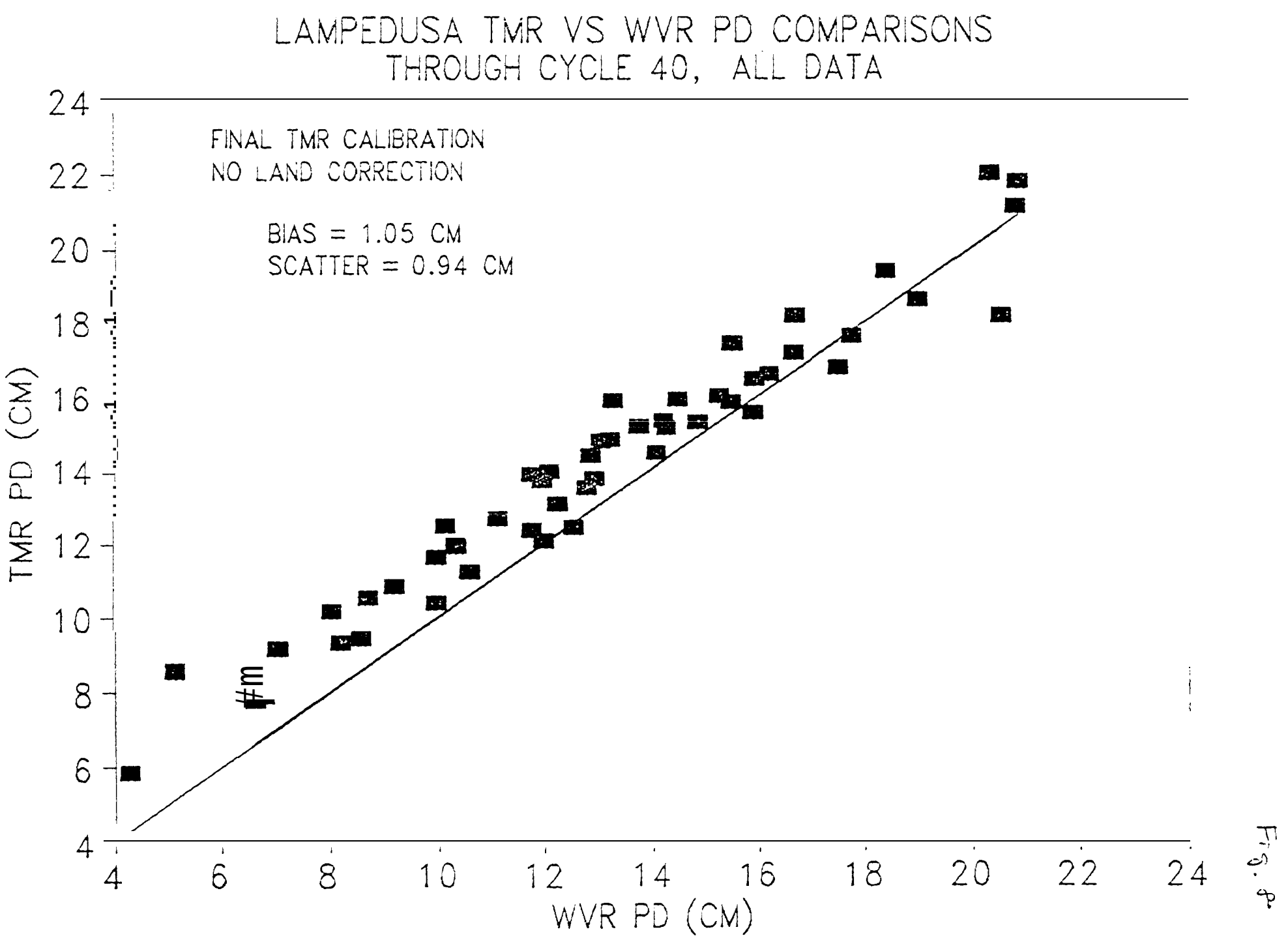
LAMPEDUSA TMR VS WVR PD COMPARISONS
THROUGH CYCLE 40, ALL DATA
FINAL TMR CALIBRATION
NO LAND CORRECTION
BIAS = 1.05 CM
SCATTER = 0.94 CM
TMR PD (CM)
WVR PD (CM)
4
6
8
10
12
14
16
18
20
22
24

Fig. 8

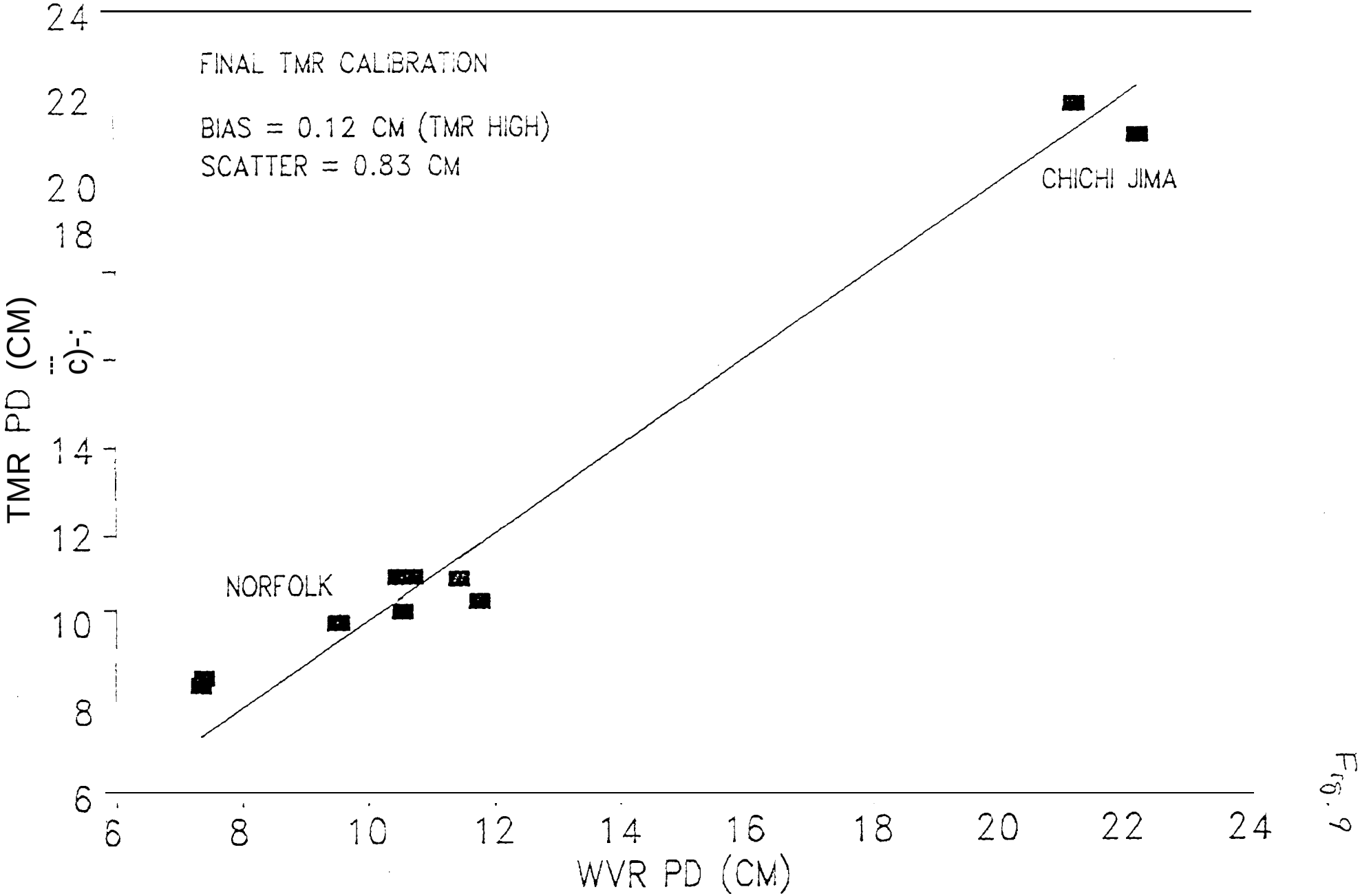
CHICHI JIMA, NORFOLK TMR—WVR PD COMPARE
10 OVERPASSES, SEP● NOV., 1992
FINAL TMR CALIBRATION
BIAS = 0.12 CM (TMR HIGH)
SCATTER = 0.83 CM
CHICHI JIMA
NORFOLK
TMR PD (CM)
WVR PD (CM)
6
8
10
12
14
16
18
20
22
24

Fig. 9